Materials & Design 249 (2025) 113538

Contents lists available at ScienceDirect

Materials & Design

journal homepage: www.elsevier.com/locate/matdes

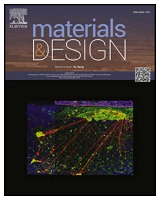

Towards a better understanding of biofoams: Multi-technique characterization of various tannin-furanic foams to assist in material selection for product design

Thomas Sepperer [a,1], Giulia Saccomano [b,c,1], Diana E. Bedolla [b,d,1], Raphael J.F. Berger [e], Primoz Šket [f], Elena Longo [b], Gregor A. Zickler [e], Saeed Borhani [e], Diego Dreossi [b], Lisa Vaccari [b], Maurizio E. Musso [e,*], Francesco D'Amico [b,*]

[a] Salzburg University of Applied Sciences, Department Green Engineering and Circular Design, Markt 136a, Kuchl 5431, Austria
[b] Elettra-Sincrotrone Trieste S.C.p.A., Strada Statale 14 – km 163,5 in AREA Science Park, Basovizza 34149, TS, Italy
[c] Department of Engineering and Architecture, University of Trieste, via Alfonso Valerio 6/1, Trieste 34127, Italy
[d] Area Science Park, Padriciano 99, Padriciano 34127, TS, Italy
[e] Paris-Lodron University of Salzburg, Department of Chemistry and Physics of Materials, Jakob-Haringer-Strasse 2a, Salzburg 5020, Austria
[f] Slovenian NMR Center, National Institute of Chemistry, Hajdrihova 19, Ljubljana SI-1000, Slovenia

A B S T R A C T

Aiming to sustainable manufacturing options, materials that are discarded from the industry and to which a second life may be given are highly desirable. Condensed tannins constitute the starting point to create tannin-furanic foams, a rigid biobased material that could be a sustainable alternative to those derived from fossil fuel-based chemicals. With the objective of developing novel foam production strategies, three different tannin-furanic foams, namely *mechanical*, *sulfuric* and *nitric*, were thoroughly chemically characterized, and their morphological and macroscopic properties were compared with those of commercial plastic foams made of polystyrene and of polyethylene terephthalate. Understanding the influence of the foaming method on the foam properties is of utmost importance when aiming to substitute existing, well-established products. The chemical characterization was performed by using NMR, FTIR and UV Raman, assisted by DFT quantum mechanics simulations. The morphological characterization was done by Scanning Electron Microscopy and X-ray micro-Tomography. Macroscopic characterization was done by strain–stress, thermal conductivity, and thermal gravimetric analysis. Our studies demonstrated *nitric* tannin-furanic foams as the closest to an insulating material, while *mechanical* tannin-furanic foam is more appropriate as a tough material. Overall, they prove that bio-based tannin-furanic foams appear to be a feasible green alternative to conventional plastic foams.

1. Introduction

Global warming, droughts, and the scarcity of fossil resources are pushing for biogenic and renewable alternatives to fossil fuel-based chemicals. Materials derived from fossil fuel are widely employed in the building insulation and packaging sector. According to Ref. [1], more than 11,730 kilotons of polystyrene-based building insulation materials were estimated to have been used in 2022 worldwide. Industrial foams do showcase significant drawbacks, that need to be overcome in order to transition towards sustainable alternatives. In the last past years, the scientific community developed biogenic insulation strategies and renewable cost-effective alternatives, nurturing commercial interest in this business sector [2–9].

Besides lignin [10–12], plant-derived tannin is the most interesting and promising candidate to replace phenol and phenol-like chemicals in the eco-friendly industry [13–22]. Currently, mimosa tannin (from the black wattle tree, *Acacia mearnsii*) is the most readily available source of condensed tannins for industrial application [23,24]. Polymerization of mimosa tannin with furfuryl alcohol results in a versatile, durable and robust resin [25–27]. Whilst tannin-furanic foams are predominantly formed by the simultaneous polymerization of condensed tannin and furfuryl alcohol and evaporation of an organic solvent [28,29], other methods for foam-formation do exist [4,5,30,31]. Foams can either be formed by solvent evaporation and catalysed by different acids (i.e. sulfuric acid and nitric acid, hereinafter defined as *sulfuric* and *nitric* tannin-furanic foams), defining their properties as done in Ref. [5]. They are characterized by low density (≈ 60–90 kg/m^3) and low thermal conductivity (30–40 mW/m K), but are limited by low mechanical

* Corresponding authors.
E-mail addresses: maurizio.musso@plus.ac.at (M.E. Musso), francesco.damico@elettra.eu (F. D'Amico).
[1] These authors contributed equally to this work.

https://doi.org/10.1016/j.matdes.2024.113538
Received 11 June 2024; Received in revised form 4 December 2024; Accepted 11 December 2024
Available online 12 December 2024

stability (compression resistance < 0.2 N/mm^2) and high friability [5]. Alternatively, it is possible to perform the so-called mechanical foaming, where a surfactant is introduced into the resin, replacing the blowing agent [31]. Strong mechanical agitation leads to incorporation of air or other surrounding gas into the wet resin, resulting in a stable meringue-like material, that can be dried. These foams tend to have higher density (100–350 kg/m^3), but also mechanical stability orders of magnitude greater compared to others (up to 1.0 N/mm^2) [31]. Hereinafter we refer to these foams as *mechanical* tannin furanic ones.

Whilst there are numerous excellent studies focusing on the physical and mechanical properties of this biobased material [28,32–36], exploring possible applications and advantages [37–39] and striving to advance the development in the area of biobased foams [40–42], only a few of them consider the direct comparison to foams derived from petroleum-based chemicals, like extruded or expanded polystyrene, polyurethane foams or other plastics like polyethylene terephthalate. Furthermore, it is still unclear the relation between the synthesis conditions and the chemical and morphological properties of the obtained tannin-furanic foams. In order to replace foams derived from petroleum-based chemicals, it is needed to gain better understanding of the possibilities to tailor the biobased foam design to specific application needs.

In the present study, tannin-furanic foams produced by different synthesis routes were thoroughly investigated. The foams here considered, namely *sulfuric*, *nitric* and *mechanical*, have been already reported for their outstanding behaviour or as important steps in the development of this material [5,31]. *Sulfuric* depicts the formaldehyde-free synthesis of tannin-furanic foams, dealing with the major issue of eliminating harmful chemicals, like formaldehyde, from synthesis [43]. Conversely, *nitric* was reported to have a relatively high compression resistance, dealing with the issue of stability [5] presented by *sulfuric*. Furthermore, ambient temperature foaming is possible for *nitric*. Lastly, *mechanical* marked a new era by presenting tannin-furanic foams with high compression resistance (up to 1 N/mm^2) and better processability of the final product, due to lower friability compared to *nitric* and *sulfuric* [31].

The shape and size uniformity of the pores formed in the foams were evaluated correlating the constitution of the tannin poly(furfuryl) alcohol (PFA) co-polymer chains formed in the polymerization, and exploring the relationship between microscopic features and macro-mechanical properties. Additionally, the influence of surfactant and other pore-shaping additives on the chemical profile of the tannin-furanic polymer was investigated. These foams were chemically characterized by using Nuclear Magnetic Resonance (NMR), Fourier Transformed Infrared spectroscopy (FTIR) and UV Resonance Raman spectroscopy (UVRR) assisted by Density Functional Theory (DFT) quantum mechanics modelling. On the other hand, the morphological and mechanical properties were also assessed using Scanning Electron Microscopy (SEM), Thermal Gravimetric Analysis (TGA), micro FTIR imaging (μ-FTIR) and X-ray micro-Tomography and compared with two commercially available plastic foams, one being expanded polystyrene (Austrotherm XPS TOP 30 SF [44]), hereinafter referred as *Ex-PS*, mainly used as thermal insulator, and the other one being recycled polyethylene terephthalate (ArmaForm PET/W GR135 [45]), hereinafter referred as *R-PET,* mainly used as building material.

To the best of our knowledge, here we provide the first comprehensive comparison and thorough characterization of biogenic foams by exploiting a multi-technique approach that provides a holistic view of tannin-furanic foams and their plastic counterparts. Overall, the results here reported shed light on the influence of synthesis procedure of tannin-furanic foams on their chemical, morphological and mechanical properties, helping identifying possible application scenarios by comparing the aforementioned properties with those of two commercially available polymer foams, in order to provide the bases to product developers and designers for the best selection of polymeric foams for various applications. Indeed, knowing materials properties and viable sustainable alternatives to established products is becoming more and more important for both product designers and material producers, as the demand for such alternatives is constantly rising [46,47].

2. Materials and methods

Tannin-furanic foams and polymers investigated in this study were produced according to the literature [5,31]. The exact compositions and associated literature references from which the formulation is taken from are shown in Table 1 with values in weight %. Three tannin-furanic foams, referred in the following as *mechanical, sulfuric*, and *nitric*, as well as three variations of the first one as mechanically foamed polymer (namely *pristine*, *Poly80* and *DEG*), were produced. *Mechanical* was produced as done in Ref. [31], *sulfuric* and *nitric* as in Ref. [5]. *Pristine*, *Poly80* and *DEG* foams were produced without the blowing agent with the same procedure as for the *mechanical* tannin-furanic foam, but with different surfactants (see Table 1). None of these three foams undergoes the formation of a proper rigid structure. A schematic representation of the foaming process is shown in Fig. 1, the detailed description of the synthesis steps is reported in Section 2 of Supplementary Material. Photos of *mechanical*, *sulfuric* and *nitric* foams are shown in Fig. S3 of Supplementary Material. The photos show a morphological homogeneity up to a mm length-scale. SEM images (Fig. S4 and S5 in Supplementary Material) evidence the presence of microstructures with dimensions lower than ≈ 250 μm, above this value the foams could be considered as homogenous. Compression resistance, density, thermal conductivity, were measured as done in Ref. [5], details including TGA being described in Supplementary Material, Section 2d.

Scanning electron microscopy (SEM) imaging of the tannin-furanic foams (*mechanical*, *sulfuric*, *nitric*) and the industrial foams (*Ex-PS* and *R-PET*) was done using a Zeiss Ultra Plus field emission scanning electron microscope equipped with an InLens secondary electron detector (Carl Zeiss AG, Oberkochen, Germany). The acceleration voltage was set to 3 kV and the working distance was adjusted between 4 and 6 mm. Before imaging, the samples were coated with a thin layer of gold using a sputter coater with a current of 40 mA and a coating time of 90 s.

X-ray phase-contrast micro-Tomography (μ-CT) scans of the above mentioned samples were performed at the SYRMEP beamline [48,49] of Elettra Sincrotrone Trieste (Italy). The beam properties of synchrotron radiation at SYRMEP beamline allow to produce high-contrast and high-resolution 3D maps of the internal micro-architecture of tannin-furanic foams. All parameters used and the complete μ-CT analysis procedure is reported in Section 5 of Supplementary Material.

Thermogravimetric analysis (TGA) was performed using a NETZSCH STA 449 F3 Jupiter instrument over a temperature range of 20 °C to 1000 °C at a heating rate of 10 °C/min, under a synthetic air atmosphere.

UV resonance Raman measurements were performed at the IUVS beamline of the Elettra Sincrotrone Trieste, a detailed description of the experimental setup being reported elsewhere [50]. Spectra acquisition and data analysis have been performed as done in Ref. [51]. Theoretical modelling has been done as carried out in Ref. [51], but using hybrid B3LYP DFT functional instead of BP86.

^{1}H–^{13}C CP-MAS NMR spectra of solid samples were recorded at the Slovenian NMR Center with a Bruker Avance NEO 400 MHz NMR (Bruker BioSpin, Rheinstetten, Germany) spectrometer equipped with 4 mm CP-MAS probe. All samples were spun at the magic angle with 10 kHz at 25 °C. The ^{1}H–^{13}C CP-MAS NMR experiments consisted of excitation of protons with a 90° pulse (P1) of 3.5 μs, CP block of 2 ms, and signal acquisition with high-power proton decoupling. A total of 13,312 scans were accumulated with a repetition delay of 3 s. The chemical shifts were referenced externally using adamantine. Prediction of ^{13}C chemical shifts was performed using ACD/NMR Predictor (Version 12.0) [52].

Attenuated Total Reflectance Fourier Transform InfraRed (ATR-FTIR) experiments were carried out at the SISSI-Bio beamline at Elettra Sincrotrone Trieste [53], and spectra were acquired using a nitrogen-fluxed Bruker Vertex 70 interferometer coupled to a DTGS detector,

Table 1
Amount (weight percentage, −%) of the several components used for the tannin-furanic foams synthesis.

Material [%]		Pristine	Poly80	DEG	Mechanical	Sulfuric	Nitric
Mimosa Tannin		43.3	40.4	38.2	36	36.4	38.6
Furfuryl alcohol		26.7	25	23.6	22.3	25.7	24.3
Water		12.9	12.1	11.5	10.8	15.2	14.3
Surfactant	DEG	−-	−-	11.5	10.8		
	Poly80	−-	6.5	−-	5.8	−-	1.4
Blowing agent		−-	−-	−-	−-	4.5 Diethyl ether	4.3 Pentane
Acid		17.1	16	15.2	14.3	18.2	17.1
		H_2SO_4 2 M	H_2SO_4 2 M	H_2SO_4 2 M	H_2SO_4 2 M	H_2SO_4 4 M	HNO_3 4 M
Reference					[31]	[5]	[5]

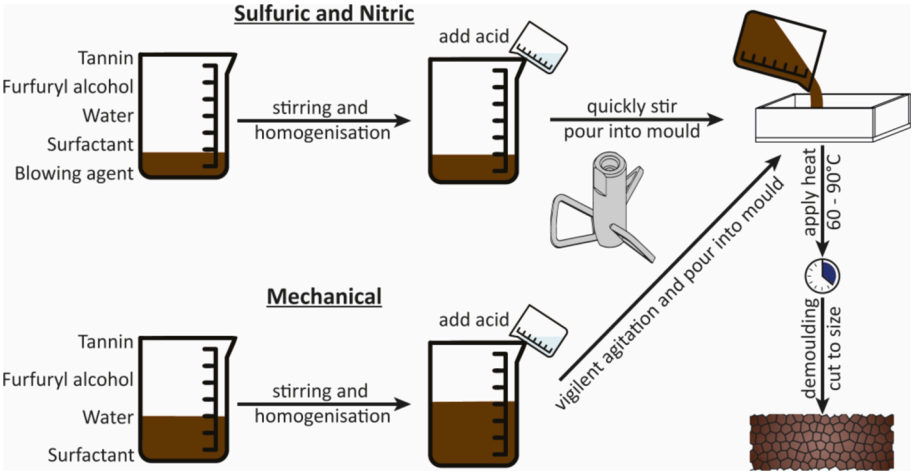

Fig. 1. Schematic representation of the *sulfuric, nitric* (top) and *mechanical* (bottom) tannin-furanic foam synthesis.

with a single reflection diamond ATR setup (Miracle, by Pike Inc). A reference spectrum was collected on the clean crystal and then a spectrum of the sample was acquired. Spectra were recorded averaging 128 scans within a spectral range of 5000–600 cm^{-1} with a spectral resolution (FWHM) of 4 cm^{-1}. Spectra were area normalized over the whole range..

To do FTIR imaging, slices of the foam were deposited on a CaF_2 window, and the smallest fragments were chosen to be measured, since those would not saturate the signal. FTIR imaging measure were also performed at the SISSI-Bio beamline of Elettra Sincrotrone Trieste [53] in transmission mode by using a nitrogen cooled 64x64 pixels Focal Plane Array (FPA) coupled to a Bruker Hyperion 3000 Vis/IR microscope and a Bruker Vertex 70v interferometer. A matching pair of 15x Cassegrain objective/condenser was used. FTIR imaging was performed by accumulating 512 scans with a spectral resolution of 4 cm^{-1} (FWHM) in the spectral range from 4000-900 cm^{-1}.

3. Results

3.1. ATR-FTIR analysis

To infer about the chemical composition of the tannin-furanic foams, in Fig. 2 are shown the ATR-FTIR spectra of *sulfuric* (blue curve), *nitric* (red curve) and *mechanical* (green curve) tannin-furanic foams, in the wavenumber ranges of 3800–2500 cm^{-1} (panel A) and 1900–600 cm^{-1} (panel B). The spectra of mimosa tannin extract (black curve) and thermosetted PFA (violet curve) have been reported for comparison. To allow a qualitative comparison between the tannin-furanic foams spectra, these were normalized relative to the intensities of the hydroxyl band at 3000–3500 cm^{-1}. The same normalization was applied to the mimosa tannin extract spectrum. PFA, that lacks of hydroxyl band, was instead normalized relative to the carbonyl band at 1713 cm^{-1} of the *sulfuric* foam, while pure Polysorbate 80 spectrum was normalized relative to the C-H stretching band at 2900 cm^{-1} of the *mechanical* tannin-furanic foam.

Between 1400 cm^{-1} and 1800 cm^{-1} it is possible to identify many spectral features of condensed tannins (i.e 1713 cm^{-1}, 1608 cm^{-1}, 1501 cm^{-1} and 1452 cm^{-1}) [54,55]. The FTIR spectral region between 1150 cm^{-1} and 1450 cm^{-1} is characterized by several spectral features which are present in furfuryl alcohol, polyfurfuryl alcohol (PFA) and condensed tannins [51,54,56,57]. Although more spectral features belonging to PFA can be also identified (i.e. 1015 cm^{-1}, 961 cm^{-1}, 785 cm^{-1} and 733 cm^{-1}), their lower intensity in the overall FTIR spectra does not allow to get any further details over the simple recognition of the PFA presence inside the tannin-furanic foams (see for comparison the UVRR spectra in Fig. 3). It has to be highligthed the presence of a band at 1713 cm^{-1} in the tannin-furanic foam FTIR spectra (panel B of Fig. 2): since such band is not present in condensed tannins, it is reasonable to assume that these functional groups result from the furan ring opening during furfuryl alcohol polymerization [51].

Noteworthily, the main spectral features belonging to Polysorbate 80 (1094 cm^{-1}) and DEG (1053 and 1125 cm^{-1}) in the 600–1200 cm^{-1} wavenumber range seem to provide only a small contribution to the overall FTIR spectrum of the *mechanical* tannin-furanic foam (see also in Supplementary Material Fig. S8). Conversely, in the FTIR spectral region between 2800 and 3000 cm^{-1} the *mechanical* tannin-furanic foam is characterized by strong absorption bands at 2855 cm^{-1}, 2870 cm^{-1} and 2920 cm^{-1}, more intense with respect to those observed in *sulfuric* and *nitric* acid prepared tannin-furanic foams (see inset in Panel A of Fig. 2). These results might be indicative of unreacted Polysorbate 80 and DEG still present inside the foam (see also in the Supplementary Material Panel B in Fig. S8).

3.2. UVRR analysis

To infer about the chemical conformation of flavonoids and PFA

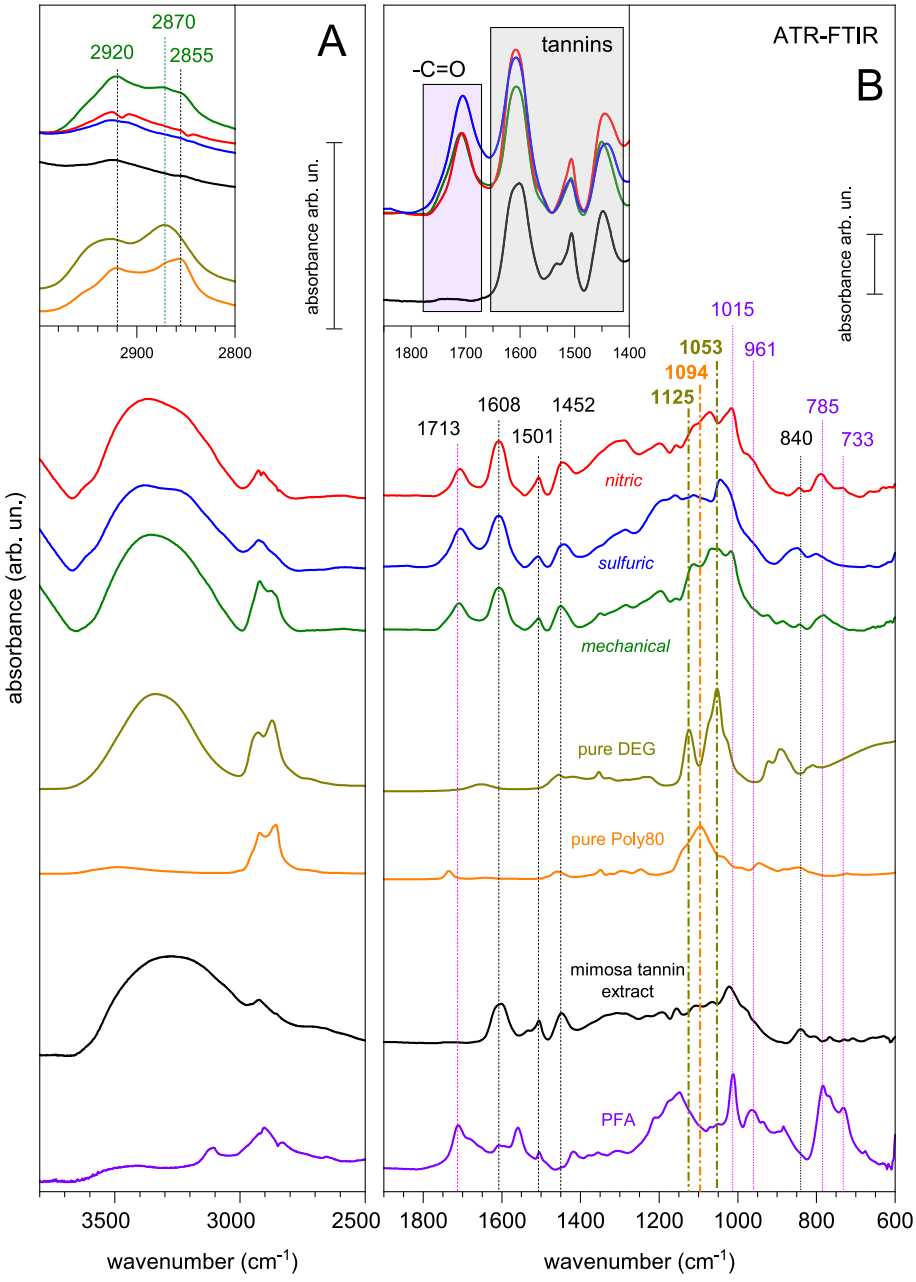

Fig. 2. Normalized ATR-FTIR spectra of *mechanical* (green curve), *sulfuric* (blue curve) and *nitric* (red curve) tannin-furanic foams in the wavenumber ranges of 3800–2500 cm^{-1} (panel A) and 1900–600 cm^{-1} (panel B). The spectra of mimosa tannin extract (black curve) and of thermosetted PFA (violet), Polysorbate 80 (yellow) and DEG (dark yellow) are reported for comparison. All spectral intensities have been normalized relative to the hydroxyl band at 3000–3500 cm^{-1}, with the exception of PFA, which is normalized relative to the carbonyl band of the *sulfuric* foam at 1713 cm^{-1}, and of Polysorbate 80, which is normalized relative to the C-H stretching band at ≈ 2900 cm^{-1}. Inset of part A compares in the 3000–2800 cm^{-1} spectral range the three types of foams with pure DEG, pure Poly80, and the mimosa tannin extract. Inset of part B is a comparison of the *nitric*, *sulfuric* and *mechanical* foams with the mimosa tannin extract in the 1800–1400 cm^{-1} spectral range.

inside tannin-furanic foams, UVRR measurements have been carried out. In UVRR the vibrational scattering coming from tannins and furan aromatic rings is resonantly enhanced, thus selectively allowing investigation of the chemical behaviour [51]. To note that measurements carried out with 532 nm and 785 nm laser excitations only produce spectra with strong fluorescence background [58].

In Panel A of Fig. 3 the UVRR spectra obtained from *mechanical* (green curve), *sulfuric* (blue curve) and *nitric* (red curve) tannin-furanic foams, collected with laser excitation source at 266 nm, are displayed in the wavenumber ranges of 500–1450 cm^{-1}, together with the UVRR spectra of PFA (violet curve), of mimosa tannin extract (brown curve), and of catechin (orange curve). In the UVRR spectra of the three tannin-furanic foams it is possible to identify the two peaks at 967 cm^{-1} and 1018 cm^{-1} characteristic of PFA [51]. No spectral features are present near this wavenumber range in the UVRR spectrum of the mimosa tannin-extract. Conversely, the two peaks present in all the tannin-furanic foams at 745 cm^{-1} and 781 cm^{-1} can be unambiguously addressed to tannins-related vibrations [55,58], as confirmed by the similarities of these peaks with the ones of mimosa tannin and catechin. It is important to note that in this UVRR spectral region PFA peaks are absent. Furthermore, for the *mechanical* tannin-furanic foam it is possible to exclude the presence of spectral contribution coming from

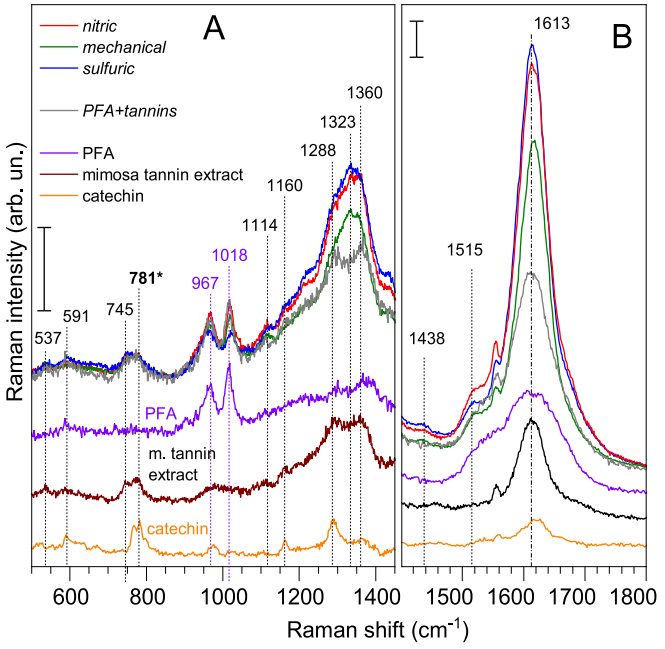

Fig. 3. Panel A; UVRR spectra of tannin-furanic foams synthesized with *mechanical* foaming (green curve), with *sulphuric* acid (blue curve) and with *nitric* acid (red curve), in the wavenumber range of 500–1450 cm^{-1}. UVRR spectra of PFA (violet), mimosa tannin extract (brown) and catechin (orange) are included for comparison. Additionally, the sum of the UVRR spectra of *PFA* and mimosa tannin extract is also reported (grey curve). Panel B; same UVRR spectra as in Panel A, but in the wavenumber range 1400–1800 cm^{-1}. The UVRR spectra have been normalized relative to the peak intensity at 781 cm^{-1}, except for PFA, normalized relative to the peak intensity at 1018 cm^{-1} of the *nitric* tannin-furanic foam.

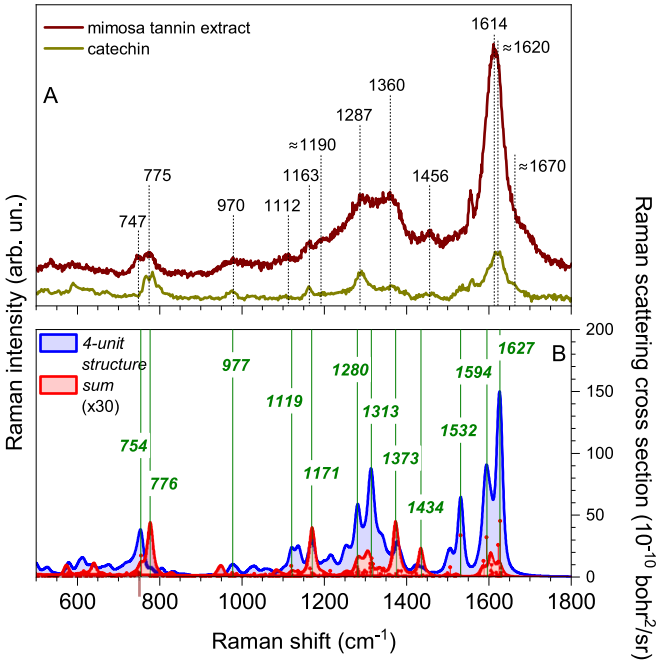

Fig. 4. Comparison among the experimental UVRR spectra of mimosa tannin extract and catechin (panel A), recorded with 266 nm excitation wavelength, and the simulated UVRR spectra (panel B) obtained from the chemical structures shown in Supplementary Material in Fig. S11, the individual simulated Raman spectra being shown in Fig. S12.

Polysorbate 80 and DEG (see in Supplementary Material Fig. S9).

The tannin-furanic foams peaks between 1100 cm^{-1} and 1400 cm^{-1} (see Fig. 3) belong to UVRR spectral regions that include contributions both from PFA and mimosa tannin extract, and a proper spectral interpretation is not trivial. Noteworthy, the panel B of Fig. 3 highlights the behaviour of the peak at 1613 cm^{-1} among the several tannin-furanic foams, compared with the analogue peak of PFA, mimosa tannin and catechin. It is possible to note that the tannin-furanic foams peaks are more intense with respect to those of mimosa tannin and catechin. A UVRR spectrum representing the sum of the UVRR spectra of *PFA* and mimosa tannin extract is also reported (grey curve in Fig. 3). To note that the 1613 cm^{-1} peak intensity in the UVRR spectra of the tannin-furanic foam is always higher than the corresponding peak in the sum spectrum. A similar behaviour occurs at 1323 cm^{-1} (Panel A of Fig. 3).

To interpret the UVRR spectral features of tannin-furanic foams belonging to tannins, specific DFT quantum mechanics simulations have been carried out, thus obtaining simulated UVRR spectral profiles to be compared with the experimental ones. In Fig. 4, the experimental 266 nm UVRR spectra of mimosa tannin and catechin (panel A) were compared (panel B) with the sum of the simulated single spectra of delphinidin, robinetinidin, cyanidin and fisietinidin, i.e. the constituents of mimosa tannin [59–61], named in the figure as *sum* (red curve), and with an oligomer composed by all these four components, here named as *4-unit structure* (blue curve), being formed by delphinidin, robinetinidin, cyanidin and fisietinidin bonded each other's via C8, C6 and C4, as indicated in Ref. [61] (see in Supplementary Material Fig. S11).

In the experimental UVRR spectrum of catechin shown in Fig. 4, the band at 775 cm^{-1} is lower, but comparable in intensity, with the one at 1614 cm^{-1} (it is roughly half intense). On the contrary, in the mimosa tannin spectrum the 1614 cm^{-1} band is much higher with respect to the one at 775 cm^{-1}. In the *sum* simulated UVRR spectrum reported in red on panel B of Fig. 4 the overall band area between 750 and 800 cm^{-1} is comparable in intensity with the one between 1550 and 1650 cm^{-1}. For the *4-unit structure* simulated UVRR spectrum (reported in blue) instead the situation changes, and this latter band becomes predominant with respect to the ones between 750 and 800 cm^{-1}. This effect indicates that this band ratio could be considered qualitatively as a fingerprint of the tannin polymerization process, i.e. more cross-linked tannin structures drive to a relevant increase of the band at around 1600 cm^{-1}.

A second spectroscopic indication of an occurring tannin structures cross-linking arises from the spectral line-shape changing between ≈ 1100 and ≈ 1450 cm^{-1} in the experimental spectrum shown in Figs. 3 and 4: while the catechin UVRR spectrum has two defined sharp peaks (namely 1160 and 1288 cm^{-1}), the mimosa tannin UVRR spectrum has a large structureless band, with broad peaks at around 1290 and 1360 cm^{-1}. This could be explained by the presence of peaks at 1280, 1313 and 1373 cm^{-1} in the *4-unit structure* simulated UVRR spectrum, which are only partially present in the *sum* simulated UVRR spectrum. This can be considered as a further indication of the mimosa tannin hetero-polymerization.

In light of the simulations, we can exploit these findings to strengthen the interpretation of the UVRR spectra of the tannin-furanic foam of Fig. 3. Since these experimental spectra are normalized to the bands at 781 cm^{-1} (a band specific of tannins), the intensity of the UVRR band at around 1613 cm^{-1} results to be indicative of the tannin polymerization degree: the higher intensity of the bands in *sulfuric* and *nitric* with respect to *mechanical* indicates that the catalytic reaction induced by the acids polymerizes better in comparison with the catalytic reaction induced by the simply mechanical process. Furthermore, the normalization carried out at 781 cm^{-1} allows to interpret the intensity changes of the bands at 967 cm^{-1} and 1018 cm^{-1} in terms of relative PFA amount [51]. From this point of view, the PFA polymerization occurs better in the *nitric* tannin-furanic foam, while the *sulfuric* one evidences a lower degree of PFA polymerization. Finally, the peak at 1323 cm^{-1} in the experimental UVRR spectra of the tannin-furanic foam of Fig. 3, which is not present in the *Tannin* + *PFA* sum spectrum reported in the same

Figure, could be further indicative of the tannin hetero-polymerization, as indicated above.

3.3. NMR analysis

Fig. 5 shows the ^{13}C NMR spectra collected from *mechanical*, *sulfuric* and *nitric* tannin-furanic foam samples. To allow spectral comparison, all the spectra have been normalized relative to their total area in the chemical shift range from δ 0 ppm to δ 260 ppm. The most important spectral variations occur below δ 90 ppm, while above δ 90 ppm only minimal variations can be detected. A summary of the peak assignments, done on the basis of experimental literature results, and of predictions done by simulations, is reported in Supplementary Material (Table S2).

It is interesting to note how the normalization carried out considering the total spectral area drives the three ^{13}C NMR spectra to have more or less the same intensity at δ 30 ppm, δ 40 ppm, $\delta \approx$ 80 ppm, $\delta \approx$ 118 ppm and $\delta \approx$ 130 ppm. In particular, the peak at δ 80 ppm belongs only to catechin atoms, specifically C2, C6 and C8, the latter two if not hydroxylated. At the same time the signal at $\approx \delta$ 118 ppm belongs to the

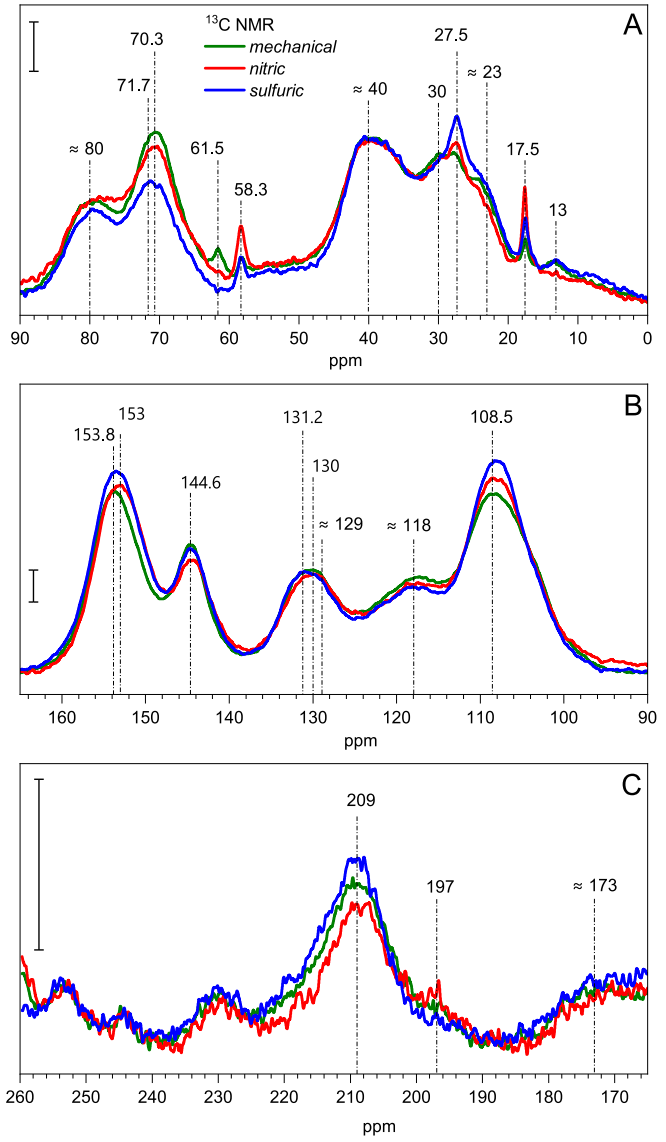

Fig. 5. Solid state 13C CP-MAS NMR of *mechanical* (green), *sulfuric* (blue) and *nitric* (red) tannin-furanic foams in the chemical shift range (panel A) δ 0–90 ppm, (panel B) δ 90–165 ppm, and (panel C) δ 165–260 ppm. Vertical bars correspond to the *y* scale units.

C1, C4′ hydroxylated and C5 not hydroxylated catechin atoms. Therefore, we can consider that the area normalization that has been carried out is very close to a normalization among the total number on flavonoid units.

Looking at Panel A of Fig. 5, we identify a signal at δ 13 ppm, present in the *mechanical* and *sulfuric* tannin-furanic foams, but not in the *nitric* one, belonging to terminal methyl groups [62]. A sharp signal at δ 17.5 and 58.3 ppm, present in all the three ^{13}C NMR spectra, could be related to the presence of residual ethanol (see in Supplementary Material Table S2). Important spectral variations occur between δ 20 and 40 ppm: the signal at δ 27.5 ppm is more intense in the *sulfuric* foam spectrum, while the signal at δ 30 ppm and the tail near δ 23 ppm have a comparable intensity in all the foams. The signal at δ 27.5 ppm could be addressed to $-CH_2-$ functional groups [62] or, alternatively, to the catechin C4 atom [63]. Instead, the signal at δ 30 ppm can be addressed to $-\underline{C}H_2-CH_2-CH_3$ [62], unreacted C4 open flavonoid unit [64], or also to $-CH_2-$ belonging to the opened rings. A comparison with the ^{13}C NMR spectra of *pristine*, *DEG* and *Poly80* tannin-furanic foams (see in Supplementary Material Fig. S13) evidences how the signals at δ 27.5 ppm and δ 30 ppm are more pronounced in the *Poly80* foam, while in the *DEG* and in the *pristine* one the signal at δ 27.5 ppm is present, but smaller. Hence, we can guess that an increase of the signal at δ 27.5 ppm implies an increase of $-CH_2-$ carbon atoms due to the presence of Polysorbate80 and DEG, or due to more ring opening processes during the foam polymerization. It is also important to note that the signal at δ 61.5 ppm is present only in the *mechanical* foam and in the *DEG* one. It can be addressed to the $-CH_2-OH$ type carbon atoms (see Ref. [4,62] and in Supplementary Material Table S2) and can be considered as fingerprint of the DEG presence inside the foam.

The signal at δ 70.3 ppm (see also Supplementary Material, Fig. S13) is predominant in the *Poly80* foam spectrum and could be reasonably assigned to the $-O-CH_2-CH_2-O-$ carbon atoms (see Ref. [62] and in Supplementary Material Table S2), although this chemical shift is also compatible with the presence of a (di)methylene-ether bridge linking two flavonoid units [59]. A similar chemical shift occurs for the C3 catechin carbon atoms, specifically simulations indicate a chemical shift of δ 66–67 ppm for isolated catechins and δ 71–72 ppm for catechins that are cross-linked via a chemical bond in C4. On the basis of this spectral interpretation, we can guess that in the *sulfuric* foam a lesser tannin polymerization degree is reached with respect to the *mechanical* and the *nitric* ones. This is compatible with the presence of $-CH_3$ residues in the *sulfuric* and not in the *nitric* foam, as indicated by the signal at δ 13 ppm. Noteworthy, the intensity of the signals around δ 70 ppm in the spectrum of the *sulfuric* tannin-furanic foam is lower with respect to the *mechanical* and *nitric* ones. This is due to the missing of Polysorbate 80 in the sulfuric foam formulation, which gives a signal at δ 70.3 ppm [62]. Significant is the absence of any signal at $\delta \approx$ 90 ppm in all the samples, indicating the lacking of catechins with R1 = OH (C6 and C8 position, see in Supplementary Material Table S2).

The spectral region between δ 180 and 220 ppm (panel C of Fig. 5) is mainly characterized by carbon atoms belonging to carbonyl groups, with the signal at δ 197 ppm more intense in the *nitric* foam spectrum than in the *mechanical* and *sulfuric* ones. Conversely, the signal at δ 209 ppm is predominant in the *sulfuric* rather than in the *nitric* tannin-furanic foam. ^{13}C NMR simulations indicate that the signal at δ 197 ppm arises from the ring opening of PFA maintaining a C = C in between the two ketones (see in Supplementary Material Fig. S14 and Table S2 and S4), while the signal at δ 209 ppm belongs to ketones coming from catechin's opened aromatic rings (see in Supplementary Material Fig. S15 and Table S2 and S5). This could be indicative of a stronger oxidation involving catechins in the *sulphuric* tannin-furanic foam, rather than in the *nitric* one, which could also explain the major fragmentation of the sulfuric polymeric structure with respect to the nitric one. In addition, the more intense signal at δ 197 ppm in the *nitric* rather than in the *sulfuric* tannin-furanic foam is indicative of a more pronounced ring opening process during the PFA polymerization in *nitric* rather than in

sulfuric foam.

3.4. μ-FTIR analysis

All the spectroscopic information obtained so far can be exploited to interpret the μ-FTIR chemical images obtained for the tannin-furanic foams. Fig. 6 shows the μ-FTIR chemical images (0.5 x 0.5 mm^2) recorded from *mechanical* (top), *sulfuric* (centre) and *nitric* (bottom) tannin-furanic foams slices. Images have been coloured by setting in red the signal coming from the 2800–3000 cm^{-1} spectral region (namely belonging to $–CH_2$ and $–CH_3$ stretching), in green the one from 1668-1760 cm^{-1} (that includes $–C = O$ stretching coming from open ring in the PFA), while the blue is defined by the 1550–1650 cm^{-1} spectral region, mainly addressing internal ring stretching within the tannin monomers. As already seen in Fig. 2, an intense signal coming from the 2800–3000 cm^{-1} region is indicative of the unreacted DEG and Polysorbate 80. Therefore, the presence of localized violet regions in the RGB *mechanical* map (superposition between $–CH_2$ and $–CH_3$ and tannin bands) indicates that the unreacted DEG and Polysorbate 80 are not homogeneously spread within the sample, but are concentrated in specific regions, further confirming their role in pore formation (see also Table 1). At the same time the separated green (PFA $–C = O$) and light blue ($C = O$ and tannins) regions on the RGB map indicate an inhomogeneous mixing between tannins and PFA. The observable spatial inhomogeneity of the chemical constitution in the *mechanical* tannin-furanic foam seems to be less present in the *sulfuric* foam. In this case, apart from small spots (coloured in red) indicative on a high local concentration of $–CH_2/–CH_3$, the chemical composition appears to be almost homogenous, although still with small inhomogeneous areas in the tannin distribution (i.e. the reader can observe well distinct green regions, characteristic of $–C = O$ PFA open rings, and blue region, characteristics of tannins). From all the three analyses, the *nitric* tannin-furanic foam appears to be the most homogenous one for a chemical perspective. It is important to highlight how the large presence in the RGB map of regions coloured in green indicates a large and spread presence of PFA chains. This is fully in accordance with the findings coming from UVRR, indicating a larger presence of PFA in the *nitric* tannin-furanic foam with respect to the *sulfuric* one.

3.5. Macroscopic properties

In Table 2 are reported the measured density, compression resistance, thermal conductivity and porosity of the tannin-furanic foam samples, along with the same parameters measured for extruded polystyrene (*Ex-PS*) foam and recycled polyethylene terephtalate foam (*R-PET*).

Commercial *Ex-PS* possesses the highest value of measured porosity, and at the same time the lowest density, and a thermal conductivity close to the lowest among the foams studied in the present work. Among the studied tannin-furanic foams, *nitric* is the one that best matches with *Ex-PS*, since it has similar porosity and thermal conductivity, while density is nearly three times higher and compression resistance is the half of *Ex-PS*. *Sulfuric* foam instead has a too low compression resistance, while *mechanical* foam, in contrast to a higher compression resistance, is too far for *Ex-PS* in terms of density (nearly 8 times above) and thermal conductivity. On the other side, *mechanical* foam results to be more similar to *R-PET*, although its density is almost twice and compression resistance is less than half that of *R-PET*.

The stress–strain curves of *mechanical*, *sulfuric* and *nitric* foams are shown in Supplementary Material (Fig. S6). According to Fig. S6, *mechanical* foam exhibits a markedly elevated compression resistance in comparison to *sulfuric* and *nitric*, reaching a value of approximately 0.9 N/mm^2 at a strain of 10 %. Conversely, *nitric* foam exhibits moderate compression resistance, increasing gradually to approximately 0.2 N/mm^2 by 10 % strain, while *sulfuric* shows the lowest compression resistance, remaining nearly flat throughout the strain range with a maximum resistance of less than 0.05 N/mm^2. These results indicate that the *mechanical* foaming process significantly enhances compression resistance of the material, while the other two foams yielded much weaker resistance under compressive strain.

The thermal degradation analysis (see Fig. S7 and Table S1 in Supplementary Material) shows how *Ex-PS* and *R-PET* degrade almost completely at a specific temperature, while for tannin-furanic foams the degradation occurs gradually by increasing temperature. This agrees with scientific literature that divides the thermal degradation of tannin-furanic foams into three stages, occurring at different temperatures. The first one ranges from room temperature to around 140 °C, where the weight loss is mostly due to water and smaller volatile organic

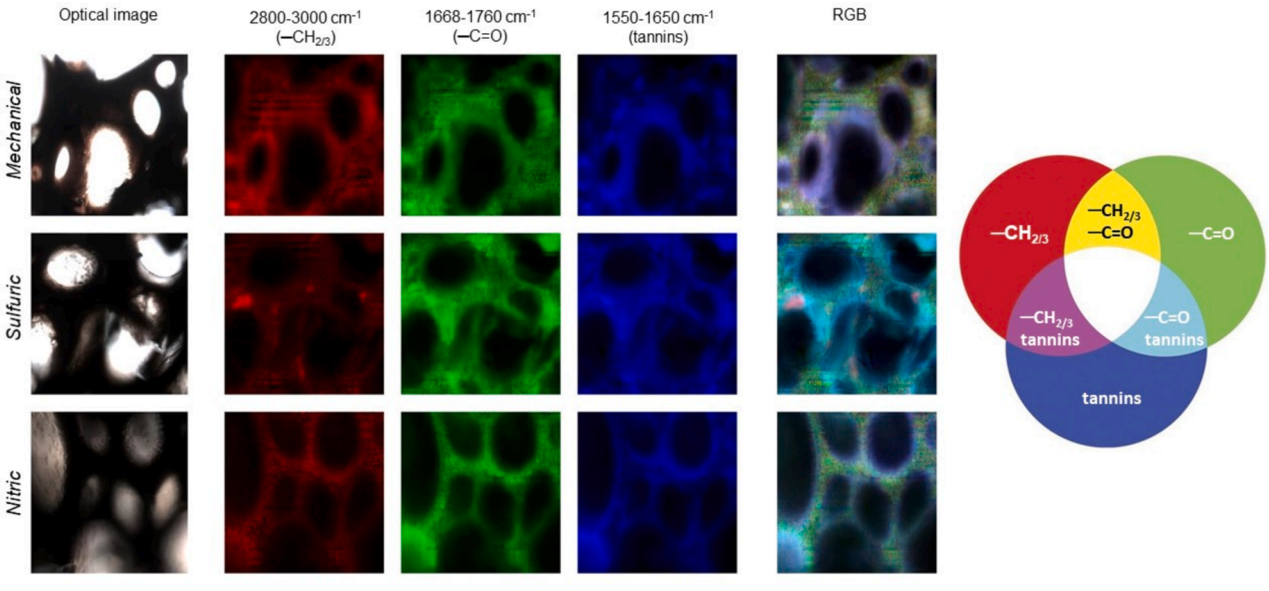

Fig. 6. μ-FTIR chemical images acquired from *mechanical* (top), *sulfuric* (center) and *nitric* (bottom) tannin-furanic foams slices. The colour maps have been selected to represent the spectral regions of 2800–3000 cm^{-1} (red), 1668–1760 cm^{-1} (green) and 1550–1650 cm^{-1} (blue). A RGB image with a combination of all the three colours is also displayed, together with a synthetic representation of its colour legend, reported on the right part of the Figure.

Table 2
Comparison among macroscopic properties for *mechanical*, *sulfuric* and *nitric* tannin-furanic foams. Macroscopic parameters for extruded polystyrene (*Ex-PS*) and recycled polyethylene terephthalate (*R-PET*) have been reported for comparison. Porosity and wall average thickness, as derived from μ-CT analysis of *mechanical*, *sulfuric, nitric, Ex-PS* and *R-PET* tannin-furanic foams, are also reported. * Values reported from the manufacturer datasheets.

		Mechanical	*Sulfuric*	*Nitric*	*Ex-PS*	*R-PET*
Macroscopic properties	Density [kg/m^3]	220 ± 11	60 ± 10	80 ± 7	29*	135*
	Compression Resistance [N/mm^2]	0.95 ± 0.08	0.05 ± 0.01	0.15 ± 0.04	0.3	2.3
	Thermal conductivity [mW/(m*K)]	45	38	32	33	37
	Porosity (from He-pycnometry, %)	86.0 ± 0.2	95.5 ± 0.7	95.3 ± 0.5	97.2	89.9
μ-CT analysis	Porosity (computed, %)	86.93	76.33	93.10	91.57	87.82
	Wall average thickness [μm]	82.45	135.73	71.07	49.52	143.09

compounds. The second stage ranges between 140 °C and 255 °C, where the decomposition of unreacted tannins starts [65]. Between 255 °C and 750 °C degradation of lateral chains of the polymer can be observed with cleavage of C-C bonds forming CO, CO_2 and CH_4 [66,67] as well as decomposition of the rigid polymer parts [66]. To derive further combustion characteristics, parameters from TG-DTG curves were used [68]. These include the ignition temperature (T_i), final burn out temperature (T_f) where 98 % are converted, maximum weight loss rate (DTG_{max}) and the corresponding temperature (T_{max}) as well as the combustibility index (S). *Mechanical* shows the lowest ignition temperature T_i (180 °C), which is comparable to many lignocellulose materials. *Nitric,* on the other hand, shows a higher ignition temperature (243 °C) and *sulfuric* the highest with 283 °C. The TGA curves show for the *sulfuric* foam a higher stability in the beginning (90 % remaining at 243 °C) while for *mechanical* and *nitric* the first 10 % weight loss is recorded at 200 °C. In contrast, the final burn out temperature T_f is much lower for *sulfuric* (600 °C) than for *nitric* (710 °C) and *mechanical* (740 °C). The difference can be explained by the different ratio of tannin to furfuryl alcohol amounts (as taken from Table 1). Whilst *sulfuric* has the lowest ratio (1.40), and therefore the highest content of furfuryl alcohol, *mechanical* and *nitric* have similar higher ratios (1.61 and 1.58). A higher amount of (poly)furfuryl alcohol leads to increased thermal stability in the beginning (degradation starts over 200 °C) and a maximum decomposition rate at around 460 °C, which is similar to the *sulfuric* sample [69]. In terms of overall combustibility, a higher value for the combustibility index S suggests a faster and better burnout [70].Whilst the two commercial plastic foams have very narrow and distinct burning properties (S of 3.69 for *Ex-PS* and 1.61 for *R-PET*), the biogenic alternatives burn out much slower (between 1.28 and 0.86), as shown in Table S1 in Supplementary Material.

3.6. X-ray μ-CT analysis

A Volume-Of-Interest (VOI) of 28.2 mm^3 was selected on the reconstructed 3D μ-CT volume for each foam sample in its most central region for the purpose of conducting a pore analysis. The motivation for the selection of the local area of the bulk interior is to avoid surface artefacts or edge effects, thereby allowing for an accurate representation of the foam's internal features, including average pore sizes, shapes, and interconnectivity. Smaller volumes of 1 mm^3 were extracted from the same VOIs and used in Fig. 7 for visualization purposes (the complete analysis workflow is shown in Supplementary Material). Images in the upper part of Fig. 7 evidence how pores differ in shape and distribution among the several samples. The *mechanical* foam shows nearly spherical cells, *sulfuric* demonstrates a variable shaping formation, and in the *nitric* foam cells show a directional expansion. The solid part of the foam decreases in quantity over the porosity because of the pore's expansion, influencing the macroscopic parameters as reported in Table 2. Commercial foams as *R-PET* exhibits thicker edges, but equally expanded pores through the volume, while *Ex-PS* exhibits minimized foam thickness while maximizing pore expansion.

Each pore extracted from the μ-CT segmentation analysis in Fig. 7 has been labelled and coloured in order to discriminate the numerosity, dimensionality and shaping properties for each foam. From the qualitative visualization perspective, mostly spherical pores are present in *mechanical* and *sulfuric* foams, while those of *nitric* appear oblique. The tomographic structural investigations highlight how industrial foams differ in a few aspects from tannin-furanic foams: *Ex-PS* has pores showing a polygonal shape, while *R-PET* has big pores, but rounded and mostly spherical. Compared to commercial foams, successful tannin-furanic foams appear to be messier, and pores are seeking expansion. This aspect is indicative of a yet-to-optimize foam-making process.

From the quantitative perspective, the equivalent pore model was

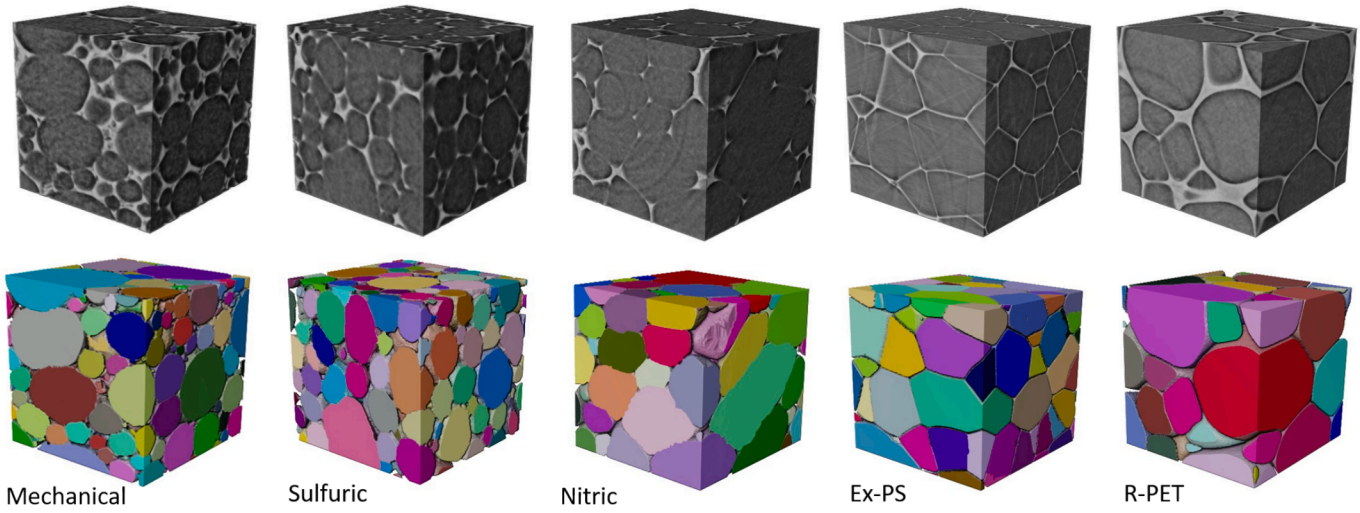

Fig. 7. 3D visualization of 1 mm^3 volume derived from μ-CT analysis of the tannin-furanic foams, from left to right *mechanical*, *sulfuric* and *nitric*, and industrial foams, *Ex-PS* and *R-PET*.The top panels reports the 3D grayscale cube and the bottom panels shows the colored pores derived from the μ-CT analysis.

carried out from μ-CT labelled data as reported in Fig. 7 and used to extract pore distribution parameters, such as the equivalent pore radius, volume, surface, and additional properties such as porosity and wall average thickness, details of this analysis is extensively reported in Supplementary Material (Tables from S6 to S8 and Figures from S17 to S20). Specifically, concerning *mechanical*, *sulfuric*, *nitric*, *Ex-PS* and *R-PET* foams, histogram distributions of pores diameter, pores surface and pores volume, and their Weibull fitting curves, have been plotted in Fig. S18, while the Weibull fitted parameters are shown in Fig. 8. The graphs show how the distribution does not follow a modal (or at least bimodal) distribution. In Fig. S19 the volume histograms express negative exponential distributions, suggesting the presence of many small pores, *Ex-PS* foam being the only exception with a curve that moves to a certain numerosity in medium dimensions of pores.

The Weibull scale parameter λ in all graphs of volume, surface area, and equivalent diameter, demonstrates that the smallest pores are in the *mechanical* foam and the biggest ones in the *Ex-PS* foam. Within the tannin-furanic foam group, *nitric* holds the largest pores. On the other hand, the Weibull shape parameter κ plots show different patterns between volume, surface area and equivalent diameter distributions. While *mechanical*, *sulfuric*, *nitric*, and *R-PET* have κ volume plots representing a monotonically decreasing pattern ($0< \kappa <1$), monotonically increasing κ-equivalent diameter plots ($\kappa >1$) are shown by *mechanical*, *sulfuric*, *nitric*, and *Ex-PS*.

When segmenting μ-CT images, *sulfuric* appears to have substantial solid parts between pores, as visible in Fig. 7. The same aspect applies to *R-PET*. Unexpectedly, even if *Ex-PS* has a thinner structure visible in Fig. 7, its porosity is smaller than the *Nitric* one. As shown in Supplementary Material in Table S8 and as inferable also from Fig. 7, *sulfuric* and *R-PET* foams show highest measurements in terms of average wall thickness, while *Ex-PS* defines the lowest value. The *nitric* foam shows the lowest resulting wall thickness compared to the other two tannin-furanic foams.

4. Discussion

All the experimental techniques adopted in this work reveal important structural and chemical differences among the prepared tannin-furanic foams. From the macroscopic point of view the *mechanical* foam sample is the one that shows the densest structure, having a density ≈ 3 times greater than the *sulfuric* and *nitric* foam samples (see Table 2). More important, its compression resistance is ≈ 20 times greater than that of the *sulfuric* sample and ≈ 6 times greater than that of the *nitric* sample, although its porosity is almost comparable with that of the *sulfuric* and *nitric* ones. However, this multi-technique investigation reveals important chemical and morphological inhomogeneities for the *mechanical* foam sample. The μ-FTIR demonstrates how the surfactant (Polysorbate 80 and DEG), included in the preparation formula to favour the bubble formation, results heterogeneously distributed inside the foam.

The situation changes when pores are produced via a blowing agent and high pressure: in this case the generated tannin-furanic foams, namely *sulfuric* and *nitric*, have lower densities and lower compression resistance with respect to the *mechanical* one. However, strong differences can be observed by comparing *sulfuric* and *nitric* foams, both in morphology and in chemical constitution. From the morphological point of view, the *sulfuric* foam recalls the *mechanical* one, although with pores average dimension slightly higher. Interestingly, for the *sulfuric* foam a strong discrepancy occurs between porosity determined by μ-CT analysis and by He pycnometry (see Table 2). To interpret this peculiar behaviour, it is important to note that the *sulfuric* foam displayed also the highest wall average thickness. Additionally, it is important to note that, for the μ-CT analysis, data were cleaned from pores with a volume smaller than 10^{-6} mm^3, it roughly means that pores with average diameter less than 10 μm could be considered as filled parts. Therefore, we can guess that the thick walls in the *sulfuric* foam actually include several small pores, not considered in the porosity calculation, resulting therefore underestimated by the μ-CT analysis. This explains both the lowest compression resistance for the *sulfuric* foam among the analysed ones, and also the discrepancy between μ-CT analysis and pycnometric measurements in the porosity evaluation.

From the chemical point of view, UVRR revealed for *sulfuric* the lowest PFA polymerization degree among the analysed tannin-furanic foams. In addition, NMR analysis points out the presence of several $–CH_3$ residues and a relevant catechin oxidation. Noteworthy, μ-FTIR shows a mild inhomogeneity in the chemical composition of *sulfuric*, with regions where the tannin presence is more pronounced, as well as with spots with high CH_2/CH_3 concentration. All these considerations suggest that the polymerization process in the *sulfuric* foam undergoes a partial fragmentation of the initial chemical constituents and does not favour a pronounced cross-linking; thus, making the final foam more fragile. This might also explain the difference in burning behaviour, as the PFA parts of *sulfuric* are more thermally stable at the beginning. From an overall point of view on the combustibility, the three tannin

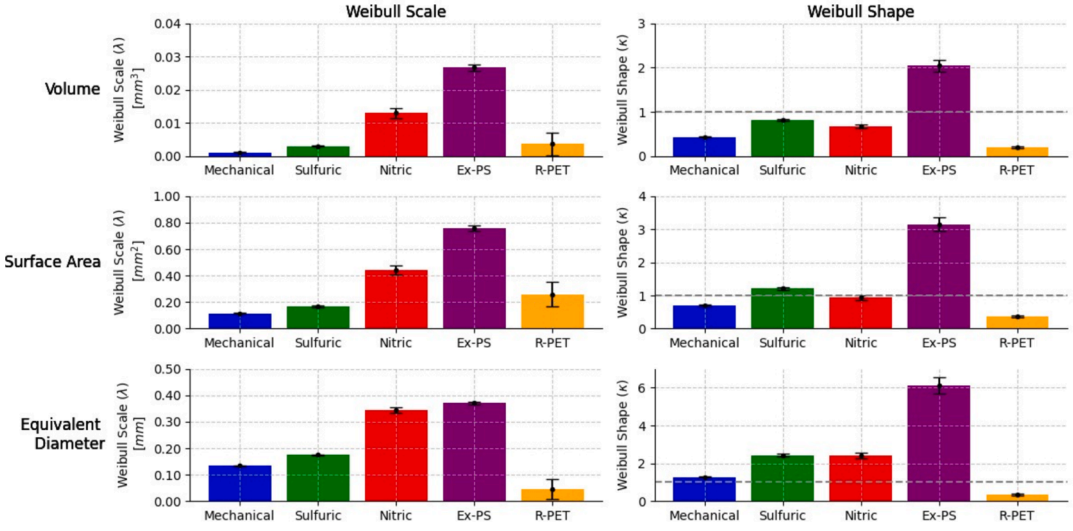

Fig. 8. Weibull scale λ and shape κ parameters obtained by fitting the pores distributions of Volume, Surface Area and Equivalent Diameter, for tannin furanic foams (*mechanical*, *sulfuric* and *nitric*) and industrial foams (*Ex-PS* and *R-PET*). For all plots, the Weibull scale λ and shape κ parameters are plotted as bar together with the C. I. of 95%. The grey dotted line in Weibull shape plots represents the unity.

foams show much lower and worst burning behaviour compared to the synthetic samples. For most applications like building insulation or fire protection, a lower S value is beneficial, as the intensity of the combustion is much weaker. Therefore, *nitric* is likely very suitable for fire protection ($S = 0.86$) followed by the two other biogenic foams (0.88 and 1.28 for *mechanical* and *sulfuric*, respectively)), and much better than *Ex-PS* which burns out quickly ($S = 3.69$).

On the contrary, the *nitric* foam results to have the most homogeneous chemical structure, as confirmed by the μ-FTIR investigation. This homogeneity is associated with a chemical composition that differs both from the *mechanical* and from the *sulfuric* foam. UVRR shows for the *nitric* foam also a high PFA polymerization degree with respect to the *sulfuric* one. This is also in accordance with the NMR and μ-FTIR analyses that show the presence of many ketones associated with open-ring PFA, homogeneously distributed inside the foam. Such a homogeneous chemical constitution possibly correlates with the pores' structure evidenced by the μ-CT analysis. Moreover, the solidity of the *nitric* tannin-furanic foam structure (higher compression resistance at a similar density compared to *sulfuric*) suggests that *nitric* foam possesses the highest degree of cross-linking among the tannin-furanic foams investigated in the present work, surely favoured by a good PFA polymerization. It is important to note that both the pores' dimensions and distribution in the *nitric* foam are better than the ones observed in commercial *R-PET* and relatively close (although still smaller) to the ones of *Ex-PS*, as well as porosity and wall average thickness.

5. Conclusions and perspectives

In the present work three tannin-furanic foams, grown by using different foaming methods and chemical formulations (namely *mechanical*, *sulfuric* and *nitric*), have been fully characterized from the structural and chemical point of view. The analyses revealed how the polymerization and bubbling formation occurring employing nitric acid, because of a good cross-linked polymerization, produced as *nitric* tannin-furanic foam the best tannin-furanic foam in terms of chemical homogeneity, low density, low thermal conductivity, and with a morphology close to the ones obtained in commercial extruded polystyrene (*Ex-PS*). All these characteristics make the *nitric* tannin-furanic foam suitable for applications as thermal insulators. On the other side the *sulfuric* tannin-furanic foam, although it possesses acceptable values of density and thermal conductivity, has a weak compression resistance and worse bubbling formation, probably due to a weak cross-linked polymerization.

The *mechanical* tannin-furanic foam morphology instead is far from the optimal one of *Ex-PS* and from the *nitric* one, and it is not homogeneous in terms of chemical constitution. However, it is characterized by an acceptable thermal conductivity (comparable to wood-fibre insulation boards) and by a compression resistance high for a bio-based foam, making it suitable as building material or core material for sandwich panels. Compared to commercially available options, *mechanical* is closest to *R-PET* and could therefore be a suitable alternative when it comes to choosing materials in the design process.

A thorough characterization of these three types of foams has demonstrated how the desired properties can be tuned and how tannin-furanic foams are suitable candidates to replace plastic foams derived from fossil fuel-based chemicals. With this study, we provide a valuable source for both designers and material producers when selecting polymeric materials for their products. It has been shown that depending on the desired use case, tannin-furanic foams are a suitable alternative to established foams and should be considered in the technical design process.

CRediT authorship contribution statement

Thomas Sepperer: Writing – review & editing, Writing – original draft, Investigation, Formal analysis, Conceptualization. **Giulia Saccomano:** Writing – review & editing, Writing – original draft, Visualization, Software, Methodology, Investigation, Formal analysis, Data curation, Conceptualization. **Diana E. Bedolla:** Writing – review & editing, Writing – original draft, Methodology, Investigation, Formal analysis, Data curation, Conceptualization. **Raphael J.F. Berger:** Writing – review & editing, Software, Methodology, Formal analysis. **Primoz Šket:** Writing – review & editing, Investigation, Formal analysis, Data curation. **Elena Longo:** Writing – review & editing, Validation, Investigation. **Gregor A. Zickler:** Data curation, Formal analysis, Investigation. **Saeed Borhani:** Data curation, Formal analysis, Investigation, Writing – review & editing. **Diego Dreossi:** Supervision, Investigation. **Lisa Vaccari:** Validation, Supervision, Funding acquisition, Writing – review & editing. **Maurizio E. Musso:** Writing – review & editing, Writing – original draft, Supervision, Funding acquisition, Conceptualization. **Francesco D'Amico:** Writing – review & editing, Writing – original draft, Supervision, Formal analysis, Data curation, Conceptualization, Investigation.

Declaration of competing interest

The authors declare that they have no known competing financial interests or personal relationships that could have appeared to influence the work reported in this paper.

Acknowledgments

The authors thankfully acknowledge financial support provided by Interreg V-A Italy–Austria 2014–2020 through the Interreg Italy–Austria project ITAT 1023 InCIMA (http://www.elettra.eu/Prj/InCIMa/) and ITAT 1059 InCIMa4 (https://www.incima4.eu/it/homepage/). The authors acknowledge also the CERIC-ERIC Consortium for providing access to access to solid state NMR facility (beamtime number 20232113), to the Elettra beamlines IUVS-OFF and SISSI-Bio (beamtime number 20217081). Work in this project was partially funded by the federal state of Salzburg in scope of the project Salzburg Center for Smart Materials 2.0 (SCSM 2.0, funding code 20102/F2300703-KZP). We acknowledge funding of the Austrian Science Fund (FWF, Fonds zur Förderung der wissenschaftlichen Forschung, project number (I 5722-N)).

Appendix A. Supplementary data

Supplementary data to this article can be found online at https://doi.org/10.1016/j.matdes.2024.113538.

Data availability

Data will be made available on request.

References

[1] Expanded Polystyrene (EPS) Market Size & Share Analysis - Industry Research Report - Growth Trends, (n.d.). https://www.mordorintelligence.com/industry-reports/global-expanded-polystyrene-eps-market-industry (accessed May 17, 2023).
[2] J. Li, J. Liao, H. Essawy, J. Zhang, T. Li, Z. Wu, G. Du, X. Zhou, Preparation and characterization of novel cellular/nonporous foam structures derived from tannin furanic resin, Ind. Crop. Prod. 162 (2021) 113264, https://doi.org/10.1016/j.indcrop.2021.113264.
[3] X. Chen, J. Li, H. Essawy, A. Pizzi, E. Fredon, C. Gerardin, G. Du, X. Zhou, Flame-retardant and thermally-insulating tannin and soybean protein isolate (SPI) based foams for potential applications in building materials, Constr. Build. Mater. 315 (2022) 125711, https://doi.org/10.1016/j.conbuildmat.2021.125711.
[4] J. Eckardt, T. Sepperer, E. Cesprini, P. Šket, G. Tondi, Comparing condensed and hydrolysable tannins for mechanical foaming of furanic foams: synthesis and characterization, Molecules 28 (2023) 2799, https://doi.org/10.3390/molecules28062799.
[5] J. Eckardt, J. Neubauer, T. Sepperer, S. Donato, M. Zanetti, N. Cefarin, L. Vaccari, M. Lippert, M. Wind, T. Schnabel, A. Petutschnigg, G. Tondi, Synthesis and characterization of high-performing sulfur-free tannin foams, Polymers 12 (2020) 564, https://doi.org/10.3390/polym12030564.

[6] C. Cazan, Advances in sustainable polymeric materials, Polymers 14 (2022) 4972, https://doi.org/10.3390/polym14224972.
[7] G.I.C. Righetti, F. Faedi, A. Famulari, Embracing sustainability: the world of bio-based polymers in a mini review, Polymers 16 (2024) 950, https://doi.org/10.3390/polym16070950.
[8] B.Y. Karlinskii, V.P. Ananikov, Recent advances in the development of green furan ring-containing polymeric materials based on renewable plant biomass, Chem. Soc. Rev. 52 (2023) 836–862, https://doi.org/10.1039/D2CS00773H.
[9] Y. Zhang, X. Liu, M. Wan, Y. Zhu, K. Zhang, From renewable biomass to bio-based epoxy monomers and bio-based epoxy curing agents: synthesis and performance, Polym. Degrad. Stab. 229 (2024) 110988, https://doi.org/10.1016/j.polymdegradstab.2024.110988.
[10] T.K. Fagbemigun, C. Mai, Production and characterisation of self-blowing lignin-based foams, Eur. J. Wood Prod. 81 (2023) 579–590, https://doi.org/10.1007/s00107-022-01908-1.
[11] Y. Yue, Y. Wang, J. Li, W. Cheng, G. Han, T. Lu, C. Huang, Q. Wu, J. Jiang, High strength and ultralight lignin-mediated fire-resistant aerogel for repeated oil/water separation, Carbon 193 (2022) 285–297, https://doi.org/10.1016/j.carbon.2022.03.015.
[12] A. Meindl, J. Grzybek, A. Petutschnigg, T. Schnabel, High purity lignin from untreated larch bark: an efficient green methodology for lignin valorization and low-value by-product mitigation, J. Wood Chem. Technol. 42 (2022) 235–243, https://doi.org/10.1080/02773813.2022.2072892.
[13] A.-K. Koopmann, J. Torres-Rodríguez, M. Salihovic, J. Schoiber, M. Musso, G. Fritz-Popovski, N. Huesing, M.S. Elsaesser, Tannin-based nanoscale carbon spherogels as electrodes for electrochemical applications, ACS Appl. Nano Mater. 4 (2021) 14115–14125, https://doi.org/10.1021/acsanm.1c03431.
[14] P. Schofield, D.M. Mbugua, A.N. Pell, Analysis of condensed tannins: a review, Anim. Feed Sci. Technol. 91 (2001) 21–40, https://doi.org/10.1016/S0377-8401(01)00228-0.
[15] A.A. Watrelot, E.L. Norton, Chemistry and reactivity of tannins in vitis spp.: a review, Molecules 25 (2020) 2110, https://doi.org/10.3390/molecules25092110.
[16] A. Arbenz, L. Avérous, Chemical modification of tannins to elaborate aromatic biobased macromolecular architectures, Green Chem. 17 (2015) 2626–2646, https://doi.org/10.1039/C5GC00282F.
[17] A.-K. Koopmann, C. Schuster, J. Torres-Rodríguez, S. Kain, H. Pertl-Obermeyer, A. Petutschnigg, N. Hüsing, Tannin-based hybrid materials and their applications: a review, Molecules 25 (2020) 4910, https://doi.org/10.3390/molecules25214910.
[18] J. Torres-Rodríguez, S.N. Myakala, M. Salihovic, M. Musso, N. Hüsing, D. Eder, V. Presser, A. Cherevan, M.S. Elsaesser, Titania hybrid carbon spherogels for photocatalytic hydrogen evolution, Carbon 202 (2023) 487–494, https://doi.org/10.1016/j.carbon.2022.10.073.
[19] T. Sepperer, A. Petutschnigg, A.-K. Koopmann, J. Torres-Rodríguez, P. Šket, D. E. Bedolla, N. Hüsing, M.S. Elsaesser, Fluorine free surface modification of tannin-furanic foams by silylation, Mater. Des. 230 (2023) 111936, https://doi.org/10.1016/j.matdes.2023.111936.
[20] K. Khanbabaee, T. van Ree, Tannins: classification and definition, Nat. Prod. Rep. 18 (2001) 641–649, https://doi.org/10.1039/B101061L.
[21] M. Pagliaro, L. Albanese, A. Scurria, F. Zabini, F. Meneguzzo, R. Ciriminna, Tannin: a new insight into a key product for the bioeconomy in forest regions, Biofuels Bioprod. Biorefin. 15 (2021) 973–979, https://doi.org/10.1002/bbb.2217.
[22] E. Cesprini, J. Jorda, M. Paolantoni, L. Valentini, P. Šket, V. Causin, D.E. Bedolla, M. Zanetti, G. Tondi, Bio-based tannin-furanic-silk adhesives: applications in plywood and chemical cross-linking mechanisms, ACS Appl. Polym. Mater. 5 (2023) 4468–4476, https://doi.org/10.1021/acsapm.3c00539.
[23] G. Tondi, M. Link, C. Kolbitsch, R. Lesacher, A. Petutschnigg, Pilot plant up-scaling of tannin foams, Ind. Crop. Prod. 79 (2016) 211–218, https://doi.org/10.1016/j.indcrop.2015.11.013.
[24] P.L. de Hoyos-Martínez, J. Merle, J. Labidi, F. Charrier El Bouhtoury, Tannins extraction: a key point for their valorization and cleaner production, J. Clean. Product. 206 (2019) 1138–1155, https://doi.org/10.1016/j.jclepro.2018.09.243.
[25] X. Li, A. Nicollin, A. Pizzi, X. Zhou, A. Sauget, L. Delmotte, Natural tannin–furanic thermosetting moulding plastics, RSC Adv. 3 (2013) 17732–17740, https://doi.org/10.1039/C3RA43095B.
[26] A.O.C. Iroegbu, S.S. Ray, On the chemistry of furfuryl alcohol polymerization: A review, Journal of Polymer Science n/a (n.d.). doi: 10.1002/pol.20230708.
[27] C. Delgado-Sánchez, F. Santiago-Medina, V. Fierro, A. Pizzi, A. Celzard, Optimisation of “green” tannin-furanic foams for thermal insulation by experimental design, Mater. Des. 139 (2018) 7–15, https://doi.org/10.1016/j.matdes.2017.10.064.
[28] G. Tondi, A. Pizzi, Tannin-based rigid foams: characterization and modification, Ind. Crop. Prod. 29 (2009) 356–363, https://doi.org/10.1016/j.indcrop.2008.07.003.
[29] C. Lacoste, M.C. Basso, A. Pizzi, M.-P. Laborie, D. Garcia, A. Celzard, Bioresourced pine tannin/furanic foams with glyoxal and glutaraldehyde, Ind. Crop. Prod. 45 (2013) 401–405, https://doi.org/10.1016/j.indcrop.2012.12.032.
[30] A. Szczurek, A. Martinez de Yuso, V. Fierro, A. Pizzi, A. Celzard, Tannin-based monoliths from emulsion-templating, Mater. Des. 79 (2015) 115–126, https://doi.org/10.1016/j.matdes.2015.04.020.
[31] T. Sepperer, P. Šket, A. Petutschnigg, N. Hüsing, Tannin-furanic foams formed by mechanical agitation: influence of surfactant and ingredient ratios, Polymers 13 (2021) 3058, https://doi.org/10.3390/polym13183058.
[32] G. Tondi, W. Zhao, A. Pizzi, G. Du, V. Fierro, A. Celzard, Tannin-based rigid foams: a survey of chemical and physical properties, Bioresour. Technol. 100 (2009) 5162–5169, https://doi.org/10.1016/j.biortech.2009.05.055.
[33] C. Lacoste, M.C. Basso, A. Pizzi, M.-P. Laborie, A. Celzard, V. Fierro, Pine tannin-based rigid foams: Mechanical and thermal properties, Ind. Crop. Prod. 43 (2013) 245–250, https://doi.org/10.1016/j.indcrop.2012.07.039.
[34] A. Celzard, W. Zhao, A. Pizzi, V. Fierro, Mechanical properties of tannin-based rigid foams undergoing compression, Mater. Sci. Eng. A 527 (2010) 4438–4446, https://doi.org/10.1016/j.msea.2010.03.091.
[35] A. Martinez de Yuso, M.C. Lagel, A. Pizzi, V. Fierro, A. Celzard, Structure and properties of rigid foams derived from quebracho tannin, Mater. Des. 63 (2014) 208–212, https://doi.org/10.1016/j.matdes.2014.05.072.
[36] F.J. Santiago-Medina, A. Tenorio-Alfonso, C. Delgado-Sánchez, M.C. Basso, A. Pizzi, A. Celzard, V. Fierro, M.C. Sánchez, J.M. Franco, Projectable tannin foams by mechanical and chemical expansion, Ind. Crop. Prod. 120 (2018) 90–96, https://doi.org/10.1016/j.indcrop.2018.04.048.
[37] A. Pizzi*, Tannin-Based Biofoams-A Review, JRM 7 (1AD) 477–492. doi: 10.32604/jrm.2019.06511.
[38] J. Sánchez-Martín, J. Beltrán-Heredia, A. Delgado-Regaña, M.A. Rodríguez-González, F. Rubio-Alonso, Adsorbent tannin foams: New and complementary applications in wastewater treatment, Chem. Eng. J. 228 (2013) 575–582, https://doi.org/10.1016/j.cej.2013.05.009.
[39] H.A.M. Bacelo, S.C.R. Santos, C.M.S. Botelho, Tannin-based biosorbents for environmental applications – A review, Chem. Eng. J. 303 (2016) 575–587, https://doi.org/10.1016/j.cej.2016.06.044.
[40] A. (Tony) Pizzi, A. Celzard, V. Fierro, G. Tondi, Chemistry, morphology, microtomography and activation of natural and carbonized tannin foams for different applications, Macromol. Symp. 313–314 (2012) 100–111, https://doi.org/10.1002/masy.201250311.
[41] M. Letellier, J. Macutkevic, A. Paddubskaya, A. Plyushch, P. Kuzhir, M. Ivanov, J. Banys, A. Pizzi, V. Fierro, A. Celzard, Tannin-based carbon foams for electromagnetic applications, IEEE Trans. Electromagn. Compat. 57 (2015) 989–995, https://doi.org/10.1109/TEMC.2015.2430370.
[42] G. Sabathi, A. Reyer, N. Cefarin, T. Sepperer, J. Eckardt, J. Neubauer, F. J. Wendisch, F. D’Amico, L. Vaccari, G. Tondi, M. Musso, Tannin-furanic foams used as biomaterial substrates for SERS sensing in possible wastewater filter applications, Mater. Res. Express 8 (2021) 115404, https://doi.org/10.1088/2053-1591/ac3586.
[43] M.C. Basso, X. Li, V. Fierro, A. Pizzi, S. Giovando, A. Celzard, Green, formaldehyde-free, foams for thermal insulation, Adv. Mater. Lett. 2 (2011) 378–382, https://doi.org/10.5185/amlett.2011.4254.
[44] Austrotherm XPS TOP 30 SF | Austrotherm - Dämmstoffe, XPS, Bauplatte, (n.d.). https://www.austrotherm.at/produkte/austrotherm-xps/austrotherm-xps-top-30-sf (accessed September 1, 2023).
[45] ArmaPET - ArmaFORM PET, (n.d.). https://local.armacell.com/en/armapet/ (accessed September 1, 2023).
[46] E.-M. Vătămănescu, D.-C. Dabija, P. Gazzola, J.G. Cegarro-Navarro, T. Buzzi, Before and after the outbreak of Covid-19: Linking fashion companies’ corporate social responsibility approach to consumers’ demand for sustainable products, J. Clean. Prod. 321 (2021) 128945, https://doi.org/10.1016/j.jclepro.2021.128945.
[47] Research: Consumers’ Sustainability Demands Are Rising, (n.d.). https://hbr.org/2023/09/research-consumers-sustainability-demands-are-rising (accessed November 8, 2024).
[48] C. Dullin, F. di Lillo, A. Svetlove, J. Albers, W. Wagner, A. Markus, N. Sodini, D. Dreossi, F. Alves, G. Tromba, Multiscale biomedical imaging at the SYRMEP beamline of Elettra – Closing the gap between preclinical research and patient applications, Phys. Open 6 (2021) 100050, https://doi.org/10.1016/j.physo.2020.100050.
[49] E. Longo, A. Contillo, L. D’Amico, M. Prašek, G. Saccomano, N. Sodini, C. Dullin, D. Dreossi, G. Tromba, SYRMEP beamline: state of the art, upgrades and future prospects, Eur. Phys. J. plus 139 (2024) 880, https://doi.org/10.1140/epjp/s13360-024-05489-1.
[50] F. D’Amico, M. Saito, F. Bencivenga, M. Marsi, A. Gessini, G. Camisasca, E. Principi, R. Cucini, S. Di Fonzo, A. Battistoni, E. Giangrisostomi, C. Masciovecchio, UV resonant raman scattering facility at Elettra, Nucl. Instrum. Methods Phys. Res., Sect. A 703 (2013) 33–37, https://doi.org/10.1016/j.nima.2012.11.037.
[51] F. D’Amico, M.E. Musso, R.J.F. Berger, N. Cefarin, G. Birarda, G. Tondi, D. Bertoldo Menezes, A. Reyer, L. Scarabattoli, T. Sepperer, T. Schnabel, L. Vaccari, Chemical constitution of polyfurfuryl alcohol investigated by FTIR and Resonant Raman spectroscopy, Spectrochim. Acta A Mol. Biomol. Spectrosc. (2021) 120090, https://doi.org/10.1016/j.saa.2021.120090.
[52] NMR Software | Processing, Prediction, and Assignment, ACD/Labs (n.d.). https://www.acdlabs.com/solutions/nmr-spectroscopy/ (accessed April 22, 2024).
[53] S. Lupi, A. Nucara, A. Perucchi, P. Calvani, M. Ortolani, L. Quaroni, M. Kiskinova, Performance of SISSI, the infrared beamline of the ELETTRA storage ring, J. Opt. Soc. Am. B 24 (2007) 959–964, https://doi.org/10.1364/JOSAB.24.000959.
[54] N. Cefarin, D.E. Bedolla, A. Surowka, S. Donato, T. Sepperer, G. Tondi, D. Dreossi, N. Sodini, G. Birarda, L. Vaccari, Study of the spatio-chemical heterogeneity of tannin-furanic foams: from 1D FTIR spectroscopy to 3D FTIR micro-computed tomography, Int. J. Mol. Sci. 22 (2021) 12869, https://doi.org/10.3390/ijms222312869.
[55] A. Ricci, K.J. Olejar, G.P. Parpinello, P.A. Kilmartin, A. Versari, Application of fourier transform infrared (FTIR) spectroscopy in the characterization of tannins, Appl. Spectrosc. Rev. 50 (2015) 407–442, https://doi.org/10.1080/05704928.2014.1000461.
[56] P. Delliere, L. Vincent, N. Sbirrazzuoli, N. Guigo, Oxygen-induced surface hardening and aromatization of thermoset furanic biobased resin: Origin and

consequences, Polym. Degrad. Stab. 230 (2024) 111020, https://doi.org/10.1016/j.polymdegradstab.2024.111020.
[57] G. Tondi, N. Cefarin, T. Sepperer, F. D'Amico, R.J.F. Berger, M. Musso, G. Birarda, A. Reyer, T. Schnabel, L. Vaccari, Understanding the polymerization of polyfurfuryl alcohol: ring opening and diels-alder reactions, Polymers 11 (2019) 2126, https://doi.org/10.3390/polym11122126.
[58] A. Reyer, G. Tondi, R.J.F. Berger, A. Petutschnigg, M. Musso, Raman spectroscopic investigation of tannin-furanic rigid foams, Vib. Spectrosc 84 (2016) 58–66, https://doi.org/10.1016/j.vibspec.2016.03.005.
[59] G. Tondi, Tannin-based copolymer resins: synthesis and characterization by solid state 13C NMR and FT-IR spectroscopy, Polymers 9 (2017) 223, https://doi.org/10.3390/polym9060223.
[60] M. Thébault, A. Pizzi1, F.J. Santiago-Medina, F.M. Al-Marzouki, S. Abdalla, Isocyanate-Free Polyurethanes by Coreaction of Condensed Tannins with Aminated Tannins, Jrm 5 (1970) 21–29. doi: 10.7569/JRM.2016.634116.
[61] H. Gerengi, K. Schaefer, H.I. Sahin, Corrosion-inhibiting effect of Mimosa extract on brass-MM55 corrosion in 0.5 M H2SO4 acidic media, J. Ind. Eng. Chem. 18 (2012) 2204–2210, https://doi.org/10.1016/j.jiec.2012.06.019.
[62] Q. Zhang, A. Wang, Y. Meng, T. Ning, H. Yang, L. Ding, X. Xiao, X. Li, NMR method for accurate quantification of polysorbate 80 copolymer composition, Anal. Chem. 87 (2015) 9810–9816, https://doi.org/10.1021/acs.analchem.5b02096.
[63] O.P. Oladosu, N.R. Isu, I.M. Aboh, S.E. Okhale, A.T. Orishadipe, H.O. Egharevba, Antibacterial activity of bioflavonoid from fruit pulps of acacia nilotica willd, Microbiology Research Journal International (2019) 1–12, https://doi.org/10.9734/mrji/2019/v28i430139.
[64] B. Zhang, A. Pizzi, M. Petrissans, A. Petrissans, C. Baptiste, Self-cross-linked tannin-aminated tannin surface coatings for particleboard, J. Renewable Mater. (2023) 1–25, https://doi.org/10.32604/jrm.2023.029761.
[65] J.M.G. Galvez, B. Riedl, A.H. Conner, Analytical Studies on Tara Tannins 51 (1997) 235–243, https://doi.org/10.1515/hfsg.1997.51.3.235.
[66] Thermogravimetric analysis of anningre tannin resin, (n.d.). https://www.scielo.cl/scielo.php?script=sci_arttext&pid=S0718-221X2016005000022&lng=en&nrm=iso&tlng=en (accessed November 21, 2024).
[67] E. Cesprini, P. Šket, V. Causin, M. Zanetti, G. Tondi, Development of Quebracho (Schinopsis balansae) Tannin-Based Thermoset Resins, Polymers 13 (2021) 4412, https://doi.org/10.3390/polym13244412.
[68] P. Jagnade, N.L. Panwar, C. Agarwal, Experimental Investigation of Kinetic Parameters of Bamboo and Bamboo Biochar Using Thermogravimetric Analysis Under Non-isothermal Conditions, Bioenerg. Res. 16 (2023) 1143–1155, https://doi.org/10.1007/s12155-022-10497-z.
[69] D.C. Odiyi, T. Sharif, R.S. Choudhry, S. Mallik, S.Z.H. Shah, A review of advancements in synthesis, manufacturing and properties of environment friendly biobased Polyfurfuryl Alcohol Resin and its Composites, Compos. B Eng. 267 (2023) 111034, https://doi.org/10.1016/j.compositesb.2023.111034.
[70] Y. Dai, M. Sun, H. Fang, H. Yao, J. Chen, J. Tan, L. Mu, Y. Zhu, Co-combustion of binary and ternary blends of industrial sludge, lignite and pine sawdust via thermogravimetric analysis: Thermal behaviors, interaction effects, kinetics evaluation, and artificial neural network modeling, Renew. Energy 220 (2024) 119610, https://doi.org/10.1016/j.renene.2023.119610.